A broadly neutralising monoclonal antibody overcomes the mutational landscape of emerging SARS-CoV2 variant of concerns

Rajesh Kumar (rajesh@thsti.res.in)

1Translational Health Science and Technology Institute, NCR Biotech Science Cluster, Faridabad 121001, Haryana, India

Hilal Parray

Translational Health Science and Technology Institute

Naveen Narayan

Regional Centre for Biotechnology

Sonal Garg

Translational Health Science and Technology Institute

Zaigham Abbas Rizvi

Translational Health Science and Technology Institute

Tripti Shrivastava

Translational Health Science and Technology Institute

Sachin Kushwaha

National Institute of Immunology

Janmejay Singh

Translational Health Science and Technology Institute

Praveenkumar Murugavelu

Translational Health Science and Technology Institute

Anbalagan Anantharaj

Translational Health Science and Technology Institute

Farha Mehdi

Translational Health Science and Technology Institute

Nisha Raj

Translational Health Science and Technology Institute

Shivam Singh

Translational Health Science and Technology Institute

Jyotsna Dandotiya

Translational Health Science and Technology Institute

Asha Lukose

Translational Health Science and Technology Institute

Deepti Jamwal
Translational Health Science and Technology Institute
Sandeep Kumar
Translational Health Science and Technology Institute
Adarsh Chiranjivi
Translational Health Science and Technology Institute
Samridhi Dhyani
Translational Health Science and Technology Institute
Nitesh Mishra
All India Institute of Medical Sciences
Kamini Jakhar
Translational Health Science And Technology Institute
Sudipta Sonar
Translational Health Science And Technology Institute
Shirlie Chowdhury
Translational Health Science and Technology Institute
Anil Panchal
Translational Health Science and Technology Institute
Manas Tripathy
Translational Health Science and Technology Institute
Shubbir Ahmed
Translational Health Science and Technology Institute
Sweety Samal
Translational Health Science and Technology Institute
Shailendra Mani
Translational Health Science And Technology Institute https://orcid.org/0000-0001-8541-8315
Sankar Bhattacharyya
Translational Health Science And Technology Institute
Supratik Das
Translational Health Science and Technology Institute
Subrata Sinha
Gaurav Batra
Translational Health Science and Technology Institute
Devinder Sehgal
National Institute of Immunology
Guruprasad Medigeshi
Translational Health Science and Technology Institute https://orcid.org/0000-0001-5333-9743
Chandresh Sharma
Translational Health Science and Technology Institute

Amit Awasthi
Translational Health Science and Technology Institute https://orcid.org/0000-0002-2563-1971
Pramod Garg
Translational Health Science and Technology Institute
Deepak Nair
Regional Centre for Biotechnology

Brief Communication

Keywords: SARS-CoV-2, Variants of concern, Omicron, Broadly neutralizing monoclonal antibody, Structure of RBD

Posted Date: March 14th, 2022

DOI: https://doi.org/10.21203/rs.3.rs-1431974/v1

Abstract

The emergence of new variants of SARS-CoV-2 necessitates unremitting efforts to discover novel therapeutic mAbs. Here, we report an extremely potent mAb named P4A2 that can neutralize all the circulating variants of concerns (VOCs) with high efficiency, including the highly transmissible Omicron. The crystal structure of the P4A2 Fab:RBD complex revealed that the residues of the RBD that interact with P4A2 are part of the ACE2-receptor-binding motif and are not mutated in any of the VOCs. The pan coronavirus pseudotyped neutralization assay confirmed that the P4A2 mAb is specific for SARS-CoV-2 and its VOCs. Passive administration of P4A2 to K18-hACE2 transgenic mice conferred protection, both prophylactically and therapeutically, against challenge with VOCs. Overall, our data shows that, the P4A2 mAb has immense therapeutic potential to neutralize the current circulating VOCs and will be highly effective against future variants as well due to its unique mode of binding.

Full Text

Existing SARS-CoV-2 vaccines and antibody therapies are rendered less effective or ineffective by newly emerging SARS-CoV-2 mutations, escalating the threat towards the human race. A recent study demonstrated that the majority of mAbs directed against Receptor-binding domain (RBD) of the SARS-CoV-2 spike protein exhibited a considerable reduction in the *in vitro* neutralising activity against the Omicron variant [1,2]. It underscores the urgent need for the development of novel broadly neutralising antibodies against the emerging variants of concern. In the present study, we generated a panel of anti-SARS-CoV-2 mAbs using mouse hybridoma technology, by immunizing BALB/c mice with purified RBD protein that corresponds to Alpha variants of SARS-CoV-2 (N501Y). The neutralization specificity of the fused hybridoma supernatants was screened, one of the mAb P4A2 demonstrated exceptional efficient and broad neutralisation of both ancestral SARS-CoV-2 WA1/2020 and other VOCs, Alpha, Beta, Kappa and Delta (range = 10-39 ng mL^{-1}) (Fig. 1A). The P4A2 binds with RBDs of different VOCs with high affinity and binding assays based on competition suggested that P4A2 binding site overlaps with the ACE2 binding site (Fig. 1B & Fig. S1).

The crystal structure of P4A2 Fab in complex with the RBD-N501Y (residues 332-544) of protein was determined to a maximum resolution of 3.0 Å (Fig. 1C). The crystal structure shows the electron density for the entire heavy and light chain of the P4A2 Fab. For the RBD, electron density for the first five residues (332-336) was disordered, and the density for residues 526-544 at the C-terminal is missing. The structure showed that the residues 475-489 and 455-456 of the RBD are present close to the P4A2 Fab paratope (Fig. 1D). The residues of the RBD that interact with the paratope of the P4A2 Fab are 455Leu, 456Phe, 483Val, 484Glu, 485Gly, 486Phe, 487Asn, and 489Tyr (Fig. 1D). The P4A2 paratope is made up of residues T30, R31, Y32, S33, Y35 and M37 from CDR1 along with N52 from CDR2 and S99 from CDR3 of the heavy chain. The residues involved from CDR1 of the light chain are Y31, T34, L36, Q38, F40 and that from CDR2 are Y53, A54, and N57. Q93 and S95 from CDR3 of the light chain also contribute to the paratope (Fig. 1D). The area of the surface buried due to interaction between RBD and P4A2 paratope is 1667 $Å^2$. The key interactions that stabilize the distributed epitopes from the Receptor-binding Motif

(RBM) in the P4A2 paratope include (i) the presence of the aromatic ring of 486Phe deep inside a hydrophobic cavity (Fig. 1E) lined by F40L, Y35H and M37H (ii) hydrogen bond formed between backbone carbonyl of R31H and backbone nitrogen of 484Glu, (iii) hydrogen bond formed between backbone carbonyl of 484Glu and backbone nitrogen of S33H, (iv) hydrogen bond formed between backbone nitrogen of 486Phe and side chain of Y35H (v) hydrogen bond formed between backbone carbonyl of 485Gly and side chain of S99H, (vi) hydrogen bond formed between side chain of 487Ser and backbone carbonyl of S95L, and (vii) hydrophobic interactions formed between 456Phe, 489Tyr, L36L and Y53L.

The residues of RBD, that interact with the paratope, are part of the RBM involved in interacting with residues of human ACE2. Based on the crystal structure of the SARS-CoV-2 RBD in complex with human ACE2 (PDB code: 6M0J), the viral protein forms interactions with the human receptor through the following residues: 417Lys, 446Gly, 449Tyr, 453Tyr, 455Leu, 456Phe, 475Ala, 486Phe, 487Asn, 489Tyr, 493Gln, 496Gly, 498Gln, 500Thr, 501Asn, 502Gly, and 505Tyr[3]. Among these residues 455Leu, 456Phe, 486Phe, 487Asn, and 489Tyr form key hydrophobic and polar interactions with the paratope of P4A2 Fab and therefore, binding of the Fab to the Spike-RBD will render these residues inaccessible to the ACE2 receptor. A superimposition of the RBD from the complex with P4A2 Fab onto that from the complex with ACE2 shows that the viral protein bound to P4A2 will be unable to engage with the human receptor due to steric clashes (Fig. 1F). The backbone conformation of the stretch spanning residues 475-488 and 455-456 from Spike-RBD is similar when bound to P4A2 and to ACE2 (6M0J) with an RMSD of 0.8 Å (Fig. 1G). Except for 486Phe which exhibits a different side chain conformation, there is substantial overlap in the side chain orientation for the other residues. The structure of the P4A2:Fab complex was utilized to generate two computational models of the Fab in complex with Spike trimer which showed that P4A2 should be able to bind to the RBD when it is both in the “up” (accessible to ACE2 receptor) or “down” (inaccessible to ACE2 receptor) positions (Fig. 1H). Overall, the composition and conformation of the epitope in RBD and the mode of binding of the Fab ensures that P4A2 interaction will prevent recognition of ACE2 by the spike protein and thus prevent entry of the virus into the host cell.

The computational models of P4A2 Fab in complex with the Spike-RBD from Beta, Gamma, Delta, Kappa and Omicron VOCs were generated. These models show that, for all the VOCs, there are no mutations in the residues that interact with the P4A2 through their side-chain. E484 is mutated to Lys, Gln or Ala in some of the VOCs, but it forms interactions with the P4A2 Fab paratope through the backbone atoms and not through the side chain. Overall, the structural analysis provides an explanation regarding the ability of the P4A2 mAb to neutralize the Alpha, Beta, Gamma, Delta, and Kappa variants and also suggests that the mutations in residues of the RBD observed in the Omicron variant will not abrogate P4A2:Spike interaction (Fig. S2). To validate this inference, we tested the neutralization potential of P4A2 with live Omicron virus. The P4A2 neutralized Omicron with an IC_{50} of 39 ng mL^{-1} (Fig. 1I), and binds to purified omicron RBD with high specificity and nanomolar affinity (Fig. 1J & K). This is further corroborated by immunofluorescence data that the number of foci recognized by P4A2 is similar in count in all the VOC-

infected cells and reveals its broad reactivity to recognize cells infected with all VOC studied (Fig. 2A, S3 and S4).

The broad-spectrum antiviral intervention effect of P4A2 against different Alpha and Beta coronaviruses was tested using vesicular stomatitis virus (VSV) pseudotyped viruses; MERS-CoV S, OC43 S, SARS-CoV S, SARS-CoV-2 S and HKU4 S, confirming that the epitope recognised by P4A2 is unique to SARS-CoV-2 family and no cross-neutralization was seen with other coronaviruses, (Fig. 2B).

We next determined whether P4A2 could confer protection *in vivo* in a K18 hACE-2 mouse challenge model of SARS-CoV-2 infection. Eight to ten-week-old animals were administered a single dose (5mg/kg) of P4A2 intraperitoneally to assess its prophylactic efficacy (against WA1/2020 SARS-CoV-2 and kappa variant) and therapeutic effect (against WA1/2020 SARS-CoV-2, kappa, Beta, and Delta). Animals were challenged intranasally with 10^5 focus-forming units (FFU) of virus. In the prophylactic group, antibody was infused one day prior to virus challenge and in therapeutic group antibody was administrated 6-8 h following infection with the virus (Fig. S5). The changes in body weight of all experimental animals were monitored on a daily basis for 6 days. Additional clinical data was analysed in order to calculate the overall disease severity index at 6-7 days post-challenge. On day 6, mice in the infection control group lost more than 10% of their body weight compared to those in the P4A2 treatment group (Fig. 2C). Furthermore, as compared to the virus challenge group, mice given P4A2 had nearly undetectable viral RNA levels in their lungs ($P<0.001$) (Fig. 2D, S6).

To determine the minimal protective dose for therapeutic protection, we next titrated the passively administered P4A2 in low dose (1 mg/kg). A 20 µg dose of the P4A2 was fully protective and sufficient to suppress viral replication in the lungs, confirming the high potency of P4A2 *in vivo* against Beta, and Delta variant (Fig. 2E, F and S7).

Few effective mAbs are currently available that neutralizes all VOCs [4]. Sotrovimab (S309) has been found to neutralise the Omicron variant, however at a significantly lesser potency than P4A2. P4A2 exhibits strong interactions with residues of RBD that are critical for binding to the ACE2 receptor. Hence, the mutations in the RBD that reduce recognition by P4A2 will also plausibly adversely impact binding to the ACE2 receptor. Therefore, the unique mode of RBD recognition employed by P4A2 will ensure that this mAb will be able to neutralize new variants that may arise in the future. Maher *et al* provide a list of predicted mutations in RBD that will reduce the efficacy of currently available therapeutic antibodies and none of these mutations should impact the ability of P4A2 to recognize the viral protein [5]. As a result, P4A2 may represent an optimal therapeutic option which is required to reduce the impact of the COVID19 pandemic on human health across the globe. Overall, our data shows that P4A2 alone is efficacious in providing protection from the tested VOC and this ability will be unaffected by future VOCs. Humanized P4A2 mAb may be used alone or in conjunction with other non-overlapping antibodies as an effective prophylactic or therapeutic strategy against current and future variants of SARS-CoV-2. Our studies with the P4A2 mAb also reinforce the idea that therapeutic molecules that bind to regions on the target protein

that are critical for natural function will be less vulnerable to loss of sensitivity due to mutations in the target protein.

Materials And Methods

Viruses and antibodies

SARS-CoV-2 to B.6, and delta lineage viruses were isolated as described previously [6,7]. Leo Poon provided SARS-CoV-2 Omicron isolate (sub-lineage BA.1) [8]. Vero E6 or Calu-3 cells were used to propagate SARS-CoV-2 variants. Dr. Raiees Andrabi (Scripps Research Institute, USA) generously provided the full-length spike proteins of SARS-CoV-1, SARS-CoV-2, MERS, HKU1, OC43, NL63, and 229E. CR3022 antibody was purchased commercially (Sino Biologicals). II62 IgG a non-neutralizing antibody was used from our previous study [9]. The pseudotyped viral stocks of all seven alpha and beta coronaviruses were prepared as described in our previous study [10]. We used B.1.1.7 (Alpha), B1.1.351 (Beta), B.1.617.1 (Kappa), B.1.617.2 (Delta) and B.1.1.529 (Omicron) terminology in throughout our manuscript.

Expression and purification of antibody and RBD protein

A synthetic codon optimized (for mammalian cells) nucleotide sequence of RBD–His (wt), spike protein (wt), and a point mutant of RBD-His (N501Y) protein (variant B.1.1.7) and RBD corresponding to other variants from SARS-CoV-2, were cloned in pcDNA3.1 plasmid vector. The constructs were expressed and produced in Expi 293 F mammalian expression system. Briefly, the cells were transiently transfected with the plasmids. The supernatant was collected after 5-6 days, and the soluble protein was purified using Ni-NTA affinity chromatography (Qiagen, Germany).

Animal ethics statement

All the mice were procured from the Small Animal Facility, THSTI, Faridabad. All animal experiments were conducted in accordance with the guidelines for the care and use of laboratory animals as promulgated by CPCSEA, Government of India and adopted by the Institution Animal Ethics Committee of THSTI (IAEC Project/Protocol No: THSTI-IAEC-146, IAEC-160). The approval of the Institutional Biosafety Committee (approval # THS-354/2021) and Department of Biotechnology Review Committee on Genetic Manipulation (RCGM approval #: BT/IBKP/137/20220) were taken before commencing work.

Generation of hybridoma for anti-RBD (N501Y) murine monoclonal antibodies

Six to eight week old, female BALB/c mice were immunized intramuscularly (I.M.) with purified RBD (N501Y) protein (30 µg in 100 µL PBS per animal) along with Quil-A adjuvant (InvivoGen, USA). Mice were boosted 3 times with the purified protein (30 µg, 15 µg and 7.5 µg in 100 µl PBS per animal), along with Quil-A adjuvant. Sera samples from mice were collected three days after the first and second booster. The mouse with the highest titer of serum cross-neutralizing antibodies, was given a final booster injection 4 days before the spleen was aseptically removed. Splenocytes were utilized in the generation of

hybridomas using ClonaCell-HY Hybridoma Generation Kit (STEMCELL Technologies, USA), in accordance with the provided protocol. The well adapted antibody secreting clones were propagated in tissue culture flasks and frozen vials of each clone were stored in liquid nitrogen for future use. Hybridoma clones secreting anti-RBD antibodies were further screened in ELISA assay.

ELISA

For the screening of hybridoma clones/ heat inactivated mice sera (Dilution starting from 1:100 to 218,700)/ purified mAbs (5 µg/ mL^{-1} to 0.002), ELISA plates were coated with recombinant RBD (N501Y) protein (1 µg mL^{-1}; 100 µL per well). Plates were blocked with 5% non-fat milk and hybridoma culture supernatant or purified mAbs were added in three fold serial dilutions. Following incubation for 1h at room temperature, goat anti-mouse-HRP conjugated secondary antibody (Jackson Immunoresearch, USA; dilution 1 in 2500) was added to each well. In case of titration experiments, purified mAbs (100 µL per well) were added as three fold serial dilutions starting with 5 µg mL^{-1}. Standard protocols of blocking (5% skimmed milk in PBS) and washing of ELISA plates (4 times with PBS-0.05% Tween-20) were followed as described previously [11,12].

Purification of anti-RBD (N501Y) murine monoclonal antibodies

Serum-free media designated for monoclonal antibody production was used to propagate the hybridoma cells (0.5×10^5 cells per mL) in a T175 tissue culture flask in order to purify the antibodies. For scale up of antibody production, a WHEATON CELLine flask was used for hybridoma culture, following the manufacturer's instructions. Protein G Agarose resin (G-Biosciences) was used to purify the anti-RBD IgG mAbs from the hybridoma culture supernatant. Five column volumes of 1X PBS were used to wash the beads in the column. Two to three column volumes of 0.1 M glycine (pH 2.5) was added to elute the antibodies, followed by neutralization with 1M Tris-HCl (pH = 8.0). The purified antibodies were dialyzed against 1X PBS three times, using dialysis tubing (Thermo Fisher Scientific, MWCO 10 kDa), and concentrated with a 50 kDa MW cut-off Amicon Ultra-15 centrifuge unit (Millipore). A 0.2 µm syringe filter (Mdi, membrane Technologies) was used to filter the antibody solutions before they could be used in experiments. NanoDrop spectrophotometer was used to estimate the protein concentration and purified IgG mAbs were visualised using 12% Tris-Glycine-SDS-PAGE analysis.

Cytopathic effect based neutralization assay

Initial screening of heat-inactivated mice serum samples and hybridoma supernatants weas performed as described [9,13], with slight modification. Briefly, heat-inactivated serum or purified mAbs were serially diluted two or four times and mixed with 100 TCID50 of SARS-CoV2 isolates. The serum or mAb mixture was transferred to the Vero E6 monolayer seeded in a 96-well plates in triplicate and incubated for 1h. The cell surface was then washed with serum-free media, and fresh complete medium was applied. The plate was further incubated for 72h at 37°C in a humidified CO_2 incubator. The cells were observed for the

absence of viral cytopathic effect and was used as an indicative of neutralization. The neutralisation titer was defined as the dilution at which no cytopathic impact was seen.

Live Virus Focus Reduction Neutralisation Assay:

Virus neutralisation assay was performed as described previously by our group [14]. Briefly, purified P4A2 antibody was twofold serially diluted starting from 20 to 0.039 µg/ mL^{-1} . The virus neutralization assay was performed in Vero E6 cells. Cells were incubated for 24 hours for Delta and 32 hours for Omicron variant. The virus stock was propagated in Calu-3 cells (American Type Culture Collection). Control purified IgG was used as experimental negative control.

Pseudovirus assay based neutralization assay

Full length spike proteins of all alpha and beta coronaviruses were co-transfected in 1.25 x 10^5 HEK293T cells, with helper plasmid expressing firefly luciferase, an HIV-1 backbone and for SARS-CoV-1 and -2, serine protease TMPRSS2 (CMV-Luc, RΔ8.2 backbone plasmid, pTMPRSS2). After 68-72h culture supernatant was collected and stored at -70°C. To access the cross- neutralization potential of P4A2, 3-fold serial dilution (starting at 10 µg mL^{-1}) of P4A2 was performed. The serially diluted P4A2 antibody was mixed with respective pseudotyped viruses for 60 minutes at 37°C. Pseudovirus/ P4A2 combinations were added to 293T-ACE2 cells pre-seeded (24h) at 20,000 cells per well. After 48–72h, relative luminescence unit (RLU) was measured on luminometer. The percent reduction in neutralization was measured as ratio of relative luminescence units (RLU) readout in the presence of P4A2 normalized to RLU readout in the absence of bnAb. Four-parameter logistic regression was used to calculate the half maximum inhibitory concentrations (IC50) (GraphPad Prism version 8.3). II62 and CR3022 mAb against SARS-CoV-2, was used as assay control.

Immunofluorescence microscopy

A 96-well plate was seeded with Vero E6 (25,000 cells per well). Virus suspensions of the indicated MOIs (100 µL per well) were added and the plate was incubated for 1 h. After 24 h incubation, cells were fixed with 7.4% formaldehyde and left overnight. Wells were washed with PBS thrice. The cells were permeabilized with 100 µL buffer (20 mM HEPES, pH 7.5, 0.1% Triton X-100, 150 mM NaCl, 5 mM EDTA, 0.02% sodium azide) at room temperature for 20 min. The cells were incubated with mAb P4A2 (diluted 1 in 2000) at room temperature for approximately 6- mins. Secondary antibody (anti-mouse Alexa 488, cat no.: A21206, Invitrogen; 100 µL diluted 1 in 500). Micro-plaques read using AID iSpot Analyzer (Autoimmun Diagnostika GmbH) and foci were counted using AID ELISPOT 8.0 software.

To check the binding of P4A2 with Delta and Omicron infected Calu 3 cells (90,000 in each well) were seeded in 8 well chamber slides. Cells were incubated for 48 h at 37°C in an incubator with supply of 5% CO_2. DMEM high glucose with 10% (v/v) fetal bovine serum (FBS) was removed 24 h later and cells were washed with 1x PBS. Cells were infected at 0.5 MOI (DMEM High glucose supplemented with 2% FBS).

Added Delta and Omicron virus (100 µL per well) and incubate at 37°C on a rocker. Removed the virus and washed twice with 1x PBS. Added 300 µL of 10 % complete DMEM and incubated for 24 h at 37 °C.

Biolayer interferometry binding assay

Binding assays were carried out using an Octet Red instrument (Forte'Bio) using biolayer interferometry (BLI), as previously described [9,15]. Briefly, mouse Fc sensors (ForteBio Inc.) were used to capture the P4A2 mAb at 10 µg mL^{-1} in 1 x kinetics buffer [1x PBS, pH 7.4, 0.01% (w/v) BSA and 0.002% (v/v) Tween-20] and incubated with different concentrations of RBD. Associations and dissociations has been reported, depending on the analyte. Data was analysed using the software ForteBio Data Analysis. The starting concentration of RBD was 300 nM followed by three-fold serial dilution.

Purification, crystallization, data collection, refinement and analysis

A total of 30 mg of P4A2 mAb was digested for Fab preparation. The Fab preparation was performed by Pierce™ Fab Preparation Kit (cat. No. 44985) as per the manufacturer protocol. The purified Fab and RBD proteins were mixed at 1:1.7 ratio and incubated overnight at 4 ℃. This was then subjected to size exclusion chromatography on 16/600 Superdex 200 column (Cytiva) in a buffer containing 20mM HEPES 7.5 and 150 mM NaCl. The peak corresponding to P4A2 Fab:RBD complex was concentrated to 10 mg mL^{-1} and stored at -80℃ by flash freezing. The purified complex was subjected to crystallization trials using commercially available screens and trays were set up using Mosquito Crystallization Robot (TTP Labtech). The hits obtained in different screens were further expanded to produce single crystals which were tested for diffraction using a METALJET X-ray home source (Bruker Inc.). The condition that provided crystals with best diffraction quality was composed of 0.2 M magnesium formate dihydrate and 10% PEG 5KMME. These crystals were frozen with 20% glycerol as cryo-protectant. X-ray diffraction data could be collected to a maximal resolution of 3.0 Å at the automated ID30A-1 beamline in ESRF, France [16]. The diffraction data was processed using IMOSFLM [17] and AIMLESS [18] programs of the CCP4 suite (Supplementary Table S1).

The structure was determined by molecular replacement using PHASER [19] and the search model was the STEC90-C11 Fab:RBD complex [20]. This model was subjected to iterative model building and refinement using COOT [21] and PHENIX [22], respectively and the sequence of the STEC90-C11 Fab was slowly changed to that of P4A2. The final R_{free} and R_{work} are 28.2 and 23.0%, respectively. The refined structure was deposited with Protein Data Bank with the accession code 7WVL.

The structure was visualized and analysed using PYMOL (Schrödinger Corp.), and the interactions were identified using the CONTACT program of CCP4 [23]. Mutations were created *in silico* in the RBD structure using PYMOL (Schrodinger Inc.) to obtain models of P4A2 Fab bound to RBD corresponding to different SARS-CoV-2 strains. These models were subjected to energy minimization using the DESMOND module of the Schrodinger suite (Schrodinger Inc.) and then analyzed. Two models of P4A2 bound to Spike Trimer with the RBD in the up and down conformation were prepared using 7TM0 [24] and 7TOU [25] and

these models were also subjected to energy minimization using the DESMOND module. All the figures were prepared using PYMOL.

Animal protection studies

Eight to ten week old K18-hACE2 transgenic mice were pebbled and randomly allotted to different groups (n = 5) *viz.,* infection control and those receiving P4A2 in different cages. The animal experiments and procedures were performed in accordance with the IAEC, IBSC and RCGM guidelines. In prophylactic treatment, antibody recipient groups were given intraperitoneal (IP) infusion of P4A2 mAb one day before challenge (day '-1'), except for the control group where PBS was given (No virus challenge). In therapeutic treatment group, the mAb was administrated 6-12 h post infection.

Clinical spectrum of SARS-CoV-2 infection

The mouse experiments were done at the Animal Biosafety Laboratory (ABSL)-3. Change in daily body weight, activity and clinical symptoms of all the animals were monitored post infection. On day 6, all the infected animals were euthanized, the lungs were collected and imaged for gross morphological studies. The Right lower lobe of the lung was immersed in a 10% (v/v) neutral formalin solution and subjected to immunohistochemistry analysis. The viral load parameters were analysed using homogenized lung tissues in a 2 mL Trizol solution. The homogenates were stored immediately at -80ºC till further use. Blood was drawn from the animals via the retro-orbital vein on days '-1' and '0', and via direct heart puncture after euthanizing the animal. Serum samples were stored at -80ºC for future experiments.

Quantification of viral load in lung

RNA was isolated from homogenised lung tissues using the Trizol-chloroform technique according to the manufacturer's procedure, and quantified using Nanodrop. Using the iScript cDNA synthesis kit (Biorad, USA) was used for cDNA synthesis. Briefly, 1 mg total RNA was reverse-transcribed into cDNA. The qPCR was performed on diluted cDNAs (1:5) using the KAPA SYBR FAST qPCR Master Mix (5x) Universal Kit (KK4600) and 7500 Dx real-time PCR equipment (Applied Biosystems, USA).The results were analysed with SDS2.1 software as previously described [26]. For virus load estimation, the CDC-approved SARS-CoV-2 N gene primers 5'-GACCCCAAAATCAGCGAAAT-3' (Forward) and 5'-TCTGGTTACTGCCAGTTGAATCTG-3' (Reverse) were used as previously described [27]. The log_{10} copy number of N gene was calculated by using pre-titrated SARS-CoV-2 genomic RNA and expressed as Log_{10} copy number/ lung mass (mg). To produce the standard curve for absolute quantification, a known copy number of viral RNA was employed as a standard.

Reverse transcriptase - polymerase chain reaction and nucleotide sequencing

The variable region of the immunoglobulin heavy and light chain genes expressed in B cell hybridoma P4A2 were PCR amplified and sequenced following the protocol and primers described previously [28]. Briefly, cDNA was synthesized from 10 to 50 snap frozen hybridoma cells, using a commercially available

kit (Qiagen, Germany) with isotype specific antisense primers, each at a concentration of 0.75 µM. The 20 µL reaction was performed at 42°C for 30 min. Reverse transcriptase was inactivated by incubating at 95°C for 3 min. The nested PCR amplification was performed using Q5 DNA polymerase (New England Labs, USA). The cDNA (4 µL) was used as template in a 50 µL first round PCR which comprised of external antisense primer (0.25 µM) and a cocktail of V_H (or V_L as the case may be) family specific external sense primers, each at a final concentration of 0.1 µM, 1 ´ Q5 DNA polymerase buffer, dNTPs (200 µM) and Q5 DNA polymerase (0.5 U) as recommended by the manufacturer. The details regarding the primers and touchdown PCR are described previously [28]. Two microliter of the first round PCR product was used as template in a 50 µL second round nested PCR following the protocol described above for the first round. The second round PCR product was column purified following the manufacturer's instructions (Invitrogen, USA) and sequenced.

Sequence analysis

The nucleotide sequence was analyzed using Sequencher (version 5.4.5; Gene Codes, USA) and MacVector (version 17.5.4; MacVector, USA) software. The V, D and J gene segment assignment was done using IMGT/V-QUEST (https://www.imgt.org/IMGT_vquest/input) [29,30] and IgBlast (https://www.ncbi.nlm.nih.gov/igblast/) [31] at default parameters.

Declarations

Authors contributions

RK, PKG and DTN designed the study. NN and DTN carried out structural analysis of the Fab:RBD complex. HAP, PKM and PV did the mice immunization experiment. CS, HAP did the hybridoma clone screening and scaling up for mAb purification. SG did all the mAb purification and characterization work with the help of RK, AL, NR, SaD and DJ. DS, SK, GB, FM and SRC did the sequencing and V(D)J gene assignment of P4A2 mAb. DS critically edited the manuscript and provided inputs in figure preparation and manuscript writing. GM, JS, AA did the Delta and Omicron neutralization experiments in FRNT assay. GM and SS also performed immunofluorescence experiments. AA, ZAR, JD performed the prophylactic and therapeutic antibody challenge experiments. TS and SK performed the BLI binding experiment, TS edited the manuscript and provided critical inputs throughout the study. AKC and SD helped in Fab preparation. SS prepared the Wuhan and Kappa virus for challenge study, SM, SB, KJ, SuS performed the CPE assay and prepared live viruses for the challenge study. MRT helped in the approval of RCGM and mice documentation for the study. SA provided the purified Beta and Gamma RBD. KL and NM did the pseudovirus neutralization assays. RK, DTN along with the inputs from PKG wrote the manuscript. KL, SuS, DS, AA and CS edited the manuscript. All authors have reviewed and approved the final version of the manuscript.

Funding Support

The work for isolation and characterization of mAbs was supported by the THSTI-Intramural grant (THSTI-DBT). Intramural funds from the Regional Centre for Biotechnology (RCB) were utilized for structural work in this study. THSTI and RCB are funded by the Department of Biotechnology, Ministry of Science and Technology, Government of India. The authors would like to thank Dr. Didier Nurizzo for help with data collection at the ID30A-1 beamline of the European Synchrotron Radiation Facility (ESRF). Data collection at the ESRF was supported by the ESRF Access Program of the Department of Biotechnology (Grant No. BT/PR36150/INF/22/214/2020).

Conflict of interest

THSTI has filled a provisional patent application in India (Indian Patent Application No. 202211005568; Filed on: February 2, 2022).

Acknowledgment

We thank Prof. Sudhanshu Vrati, Director, RCB for establishing a collaborative effort on structural aspects of broadly neutralizing mAbs. The following reagent was deposited by the Centre for Disease Control and Prevention and obtained through BEI Resources, NIAID, NIH: SARS-Related Coronavirus 2, Isolate USA-WA1/2020, NR-52281, Isolate USA/CA_CDC_5574/2020, NR-54011 and Isolate hCoV-19/South Africa/KRISP-K005325/2020, (NR-54009, contributed by Alex Sigal (CHECK) and Tulio de Oliveira), Isolate hCoV-19/USA/PHC658/2021 (Lineage B.1.617.2; Delta Variant).

References

1. Cao, Y. *et al.* Omicron escapes the majority of existing SARS-CoV-2 neutralizing antibodies. *Nature* 1–7 (2021) doi:10.1038/s41586-021-04385-3.
2. VanBlargan, L. A. *et al.* An infectious SARS-CoV-2 B.1.1.529 Omicron virus escapes neutralization by therapeutic monoclonal antibodies. *Nat Med* (2022) doi:10.1038/s41591-021-01678-y.
3. J, L. *et al.* Structure of the SARS-CoV-2 spike receptor-binding domain bound to the ACE2 receptor. *Nature* **581**, (2020).
4. Chen, Z. *et al.* Extremely potent monoclonal antibodies neutralize Omicron and other SARS-CoV-2 variants. *medRxiv* 2022.01.12.22269023 (2022) doi:10.1101/2022.01.12.22269023.
5. Maher, M. C. *et al.* Predicting the mutational drivers of future SARS-CoV-2 variants of concern. *Sci Transl Med* **14**, eabk3445 (2022).
6. Kinetics of viral load, immunological mediators and characterization of a SARS-CoV-2 isolate in mild COVID-19 patients during acute phase of infection | medRxiv. https://www.medrxiv.org/content/10.1101/2020.11.05.20226621v2.
7. Thiruvengadam, R. *et al.* Effectiveness of ChAdOx1 nCoV-19 vaccine against SARS-CoV-2 infection during the delta (B.1.617.2) variant surge in India: a test-negative, case-control study and a

mechanistic study of post-vaccination immune responses. *The Lancet Infectious Diseases* **0**, (2021).

8. Gu, H. *et al.* Probable Transmission of SARS-CoV-2 Omicron Variant in Quarantine Hotel, Hong Kong, China, November 2021. *Emerg Infect Dis* **28**, 460–462 (2022).
9. Parray, H. A. *et al.* Identification of an anti-SARS-CoV-2 receptor binding domain directed human monoclonal antibody from a naïve semi-synthetic library. *J. Biol. Chem.* (2020) doi:10.1074/jbc.AC120.014918.
10. Mishra, N. *et al. Cross-neutralization of SARS-CoV-2 by HIV-1 specific broadly neutralizing antibodies and polyclonal plasma*. http://biorxiv.org/lookup/doi/10.1101/2020.12.09.418806 (2020) doi:10.1101/2020.12.09.418806.
11. Kumar, R. *et al.* A novel strategy for efficient production of anti-V3 human scFvs against HIV-1 clade C. *BMC Biotechnol.* **12**, 87 (2012).
12. Kumar, R. *et al.* Isolation and Characterization of Cross-Neutralizing Human Anti-V3 Single-Chain Variable Fragments (scFvs) Against HIV-1 from an Antigen Preselected Phage Library. *Applied Biochemistry and Biotechnology* **187**, 1011–1027 (2019).
13. Murugavelu, P. *et al.* Non-neutralizing SARS CoV-2 directed polyclonal antibodies demonstrate cross-reactivity with the HA glycans of influenza virus. *International Immunopharmacology* **99**, 108020 (2021).
14. Sub-optimal Neutralisation of Omicron (B.1.1.529) Variant by Antibodies induced by Vaccine alone or SARS-CoV-2 Infection plus Vaccine (Hybrid Immunity) post 6-months | medRxiv. https://www.medrxiv.org/content/10.1101/2022.01.04.22268747v1.
15. Perween, R. *et al.* A rapid novel strategy for screening of antibody phage libraries for production, purification, and functional characterization of amber stop codons containing single-chain antibody fragments. *Biotechnol Prog* e3136 (2021) doi:10.1002/btpr.3136.
16. Svensson, O., Malbet-Monaco, S., Popov, A., Nurizzo, D. & Bowler, M. W. Fully automatic characterization and data collection from crystals of biological macromolecules. *Acta Crystallogr D Biol Crystallogr* **71**, 1757–1767 (2015).
17. Battye, T. G. G., Kontogiannis, L., Johnson, O., Powell, H. R. & Leslie, A. G. W. iMOSFLM: a new graphical interface for diffraction-image processing with MOSFLM. *Acta Crystallogr D Biol Crystallogr* **67**, 271–281 (2011).
18. Evans, P. R. & Murshudov, G. N. How good are my data and what is the resolution? *Acta Crystallogr D Biol Crystallogr* **69**, 1204–1214 (2013).
19. McCoy, A. J. *et al.* Phaser crystallographic software. *J Appl Crystallogr* **40**, 658–674 (2007).
20. Bertoglio, F. *et al.* A SARS-CoV-2 neutralizing antibody selected from COVID-19 patients binds to the ACE2-RBD interface and is tolerant to most known RBD mutations. *Cell Rep* **36**, 109433 (2021).
21. Emsley, P. & Cowtan, K. Coot: model-building tools for molecular graphics. *Acta Crystallogr D Biol Crystallogr* **60**, 2126–2132 (2004).

22. Liebschner, D. *et al.* Macromolecular structure determination using X-rays, neutrons and electrons: recent developments in Phenix. *Acta Crystallogr D Struct Biol* **75**, 861–877 (2019).
23. Winn, M. D. *et al.* Overview of the CCP4 suite and current developments. *Acta Crystallogr D Biol Crystallogr* **67**, 235–242 (2011).
24. McCallum, M. *et al.* Structural basis of SARS-CoV-2 Omicron immune evasion and receptor engagement. *Science* **375**, 864–868 (2022).
25. Gobeil, S. M.-C. *et al.* Structural diversity of the SARS-CoV-2 Omicron spike. *bioRxiv* 2022.01.25.477784 (2022) doi:10.1101/2022.01.25.477784.
26. Rizvi, Z. A. *et al.* High-salt diet mediates interplay between NK cells and gut microbiota to induce potent tumor immunity. *Sci Adv* **7**, eabg5016 (2021).
27. Rizvi, Z. A. *et al.* Golden Syrian hamster as a model to study cardiovascular complications associated with SARS-CoV-2 infection. *Elife* **11**, e73522 (2022).
28. Rohatgi, S., Ganju, P. & Sehgal, D. Systematic design and testing of nested (RT-)PCR primers for specific amplification of mouse rearranged/expressed immunoglobulin variable region genes from small number of B cells. *J Immunol Methods* **339**, 205–219 (2008).
29. Brochet, X., Lefranc, M.-P. & Giudicelli, V. IMGT/V-QUEST: the highly customized and integrated system for IG and TR standardized V-J and V-D-J sequence analysis. *Nucleic Acids Res* **36**, W503-508 (2008).
30. Giudicelli, V., Brochet, X. & Lefranc, M.-P. IMGT/V-QUEST: IMGT standardized analysis of the immunoglobulin (IG) and T cell receptor (TR) nucleotide sequences. *Cold Spring Harb Protoc* **2011**, 695–715 (2011).
31. Ye, J., Ma, N., Madden, T. L. & Ostell, J. M. IgBLAST: an immunoglobulin variable domain sequence analysis tool. *Nucleic Acids Res* **41**, W34-40 (2013).

Figures

A

CPE_{100} neutralization titres with live authentic SARS-CoV2 and its VOCs viruses (ng/mL)						
	WA1/2020	Kappa	Delta	Alpha	Beta	Isotype
P4A2	*39*	*39*	*39*	*10*	*39*	IgG2b
CR3022	*>5000*	*>5000*	*>5000*	*>5000*	*>5000*	
II62	*>5000*	*>5000*	*>5000*	*>5000*	*>5000*	

B

P4A2 mAb	K_d	K_{on} (1/Ms)	K_{off} (1/s)
RBD WA1/2020	$<1.0 \times 10^{-12}$	3.7×10^{5}	$<1.0 \times 10^{-7}$
RBD Alpha	$<1.0 \times 10^{-12}$	5.7×10^{5}	$<1.0 \times 10^{-7}$
RBD Beta	0.45×10^{-9}	2.6×10^{5}	1.19×10^{-4}
RBD Gamma	0.52×10^{-9}	2.7×10^{5}	1.42×10^{-4}
RBD Kappa	0.29×10^{-9}	5.6×10^{5}	1.59×10^{-4}
RBD Delta	$<1.0 \times 10^{-12}$	4.4×10^{5}	$<1.0 \times 10^{-7}$

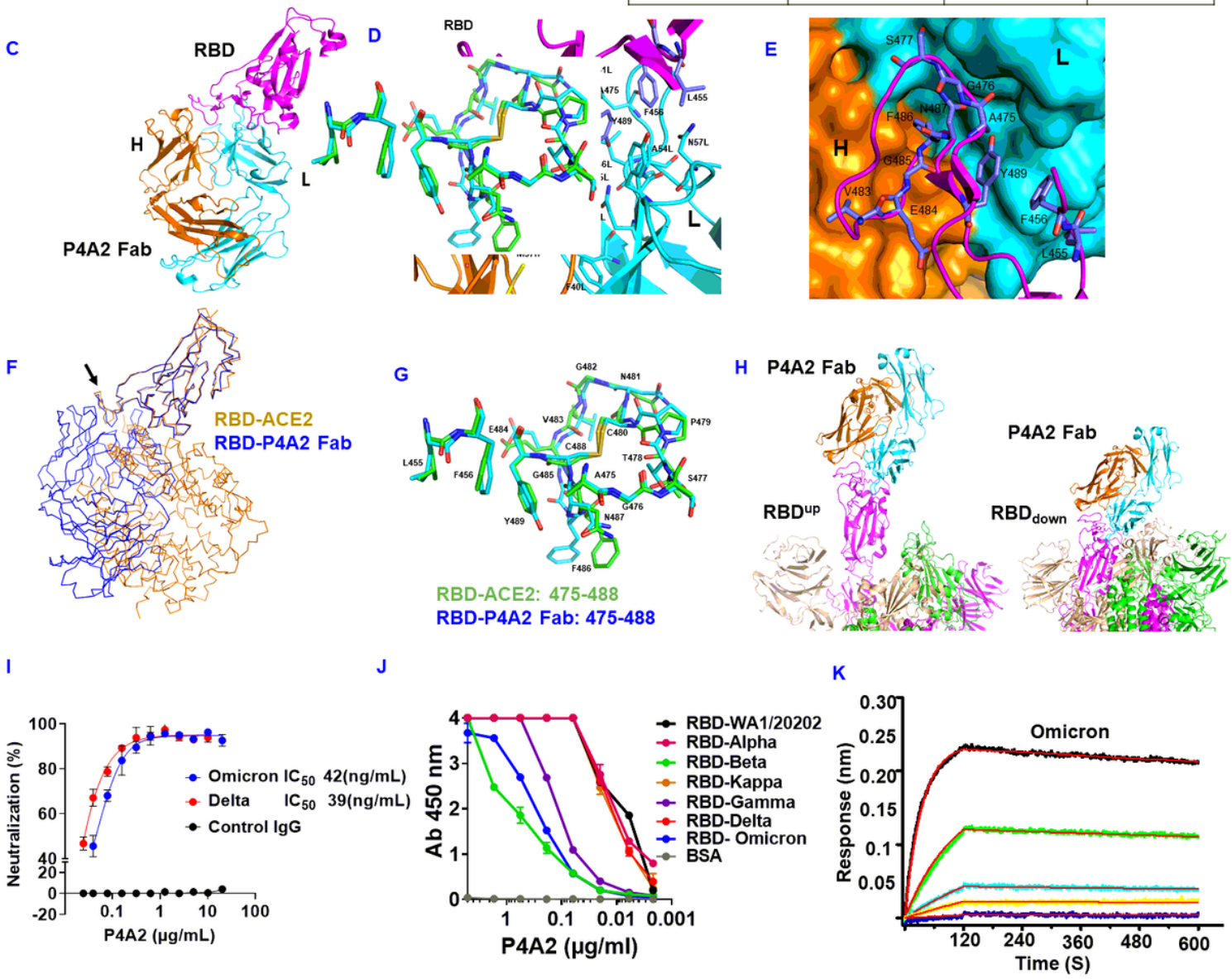

Figure 1

(A), Neutralization of authentic SARS-CoV-2 VOCs by P4A2 was determined using virus-induced cytopathic effect (CPE) based assay. (B) Kinetics of P4A2 binding to RBDs from VOC was accessed by BLI-Octet. (C) Structure of P4A2 Fab in complex with RBD of Alpha variant. The heavy (H) and light (L) chain of P4A2 Fab are coloured in orange and cyan, respectively and the RBD is coloured magenta. (D) The interacting residues from P4A2 paratope and the RBD epitope are displayed in stick representation and coloured according to element. The carbon atoms of H, L chain and RBD are coloured in yellow, cyan

and magenta, respectively. (E) Surface representation of the P4A2 paratope with the RBD epitope is shown. 486Phe from RBD is present in a hydrophobic cavity formed on the paratope. (F) Superimposition of the P4A2-Fab:RBD (green) and the ACE2:RBD structures (blue) shows that P4A2 binding to RBD will prevent interaction of the viral protein with the ACE2 receptor. (G) Superimposition of the structure of residues 475-488 and 455-456 of RBD when bound to P4A2 Fab and ACE2 receptor. The carbon atoms of this stretch when bound to Fab and ACE2 are coloured cyan and green, respectively. (H) Computational model of P4A2 Fab bound to spike trimer show that the P4A2 can bind to the RBD of the trimer in both the ACE2 receptor accessible “up” and receptor-inaccessible “down” position. (I) Neutralization of authentic SARSCoV-2 Omicron and Delta by P4A2 was determined using focus-reduction neutralization assay, (J) Binding avidity (EC50) of P4A2 to different VOCs RBD proteins were determined by ELISA, (K) Kinetics of P4A2 binding to Omicron RBD protein was accessed by BLI-Octet.

Figure 2

(A), Calu 3 cells were infected with Delta and Omicron variants of SARS CoV-2 at 0.5 MOI. At 24 h post infection, cells were fixed with chilled methanol, stained with P4A2 antibody and visualized by immunofluorescence microscopy. DAPI was used to stain nuclei. Images were captured at 10´ magnification. Representative image of uninfected cells (*First row*), Calu 3 cells infected with delta strain (*middle row*), and Calu 3 cells infected with Omicron strain of SARS CoV-2 (last row). Scale bar is 100 µm, (B), Broad spectrum cross-neutralization potential of P4A2 against Alpha and Beta coronaviruses was accessed in pseudotyped viral neutralization assay. (C, D, E, F). P4A2 offers low-dose prophylactic and therapeutic protection in the K18-hACE2 mouse model. P4A2 antibody was infused intravenously as a single dose of 100 µg (5 mg/ kg body weight) as prophylactic treatment, 24 h prior to intranasal inoculation with 10^5 PFU of SARS-CoV-2 Wuhan and Kappa isolate. (C) Body mass of mice from each group was recorded for 6 days post infection and was plotted as percent change with respect to the day 0 body mass (day of infection, dpi). (D) Lung RNA samples were used to evaluate viral load by qPCR for N gene against a known standard. The Log_{10} copy number values obtained were plotted as bar graph mean ± SEM. (E) Percent change in body mass of mice challenged with Wuhan, Kappa, Delta and Beta variants in presence or absence of therapeutic treatment of P4A2 at two different concentrations (5 mg and 1 mg of mAb per kg body mass) is plotted as a line graph till 6 dpi, (F) Log_{10} N copy number for viral load assessment from the lungs of the mice at 6 dpi. Graphs plotted represent mean ± SEM values for each group. *P < 0.05, **P < 0.01, ***P < 0.001, and ****P < 0.0001 (One-way or Two-way ANOVA).

Supplementary Files

This is a list of supplementary files associated with this preprint. Click to download.

- SupplementaryFile.docx